

Fermilab-Pub-98/232A

astro-ph/9807279

submitted to *Physical Review D***Precision Prediction for the Big-Bang Abundance of Primordial  $^4\text{He}$** Robert E. Lopez<sup>1,2</sup> and Michael S. Turner<sup>1,2,3</sup><sup>1</sup>*Department of Physics,**The University of Chicago, Chicago, IL 60637-1433*<sup>2</sup>*NASA/Fermilab Astrophysics Center,**Fermi National Accelerator Laboratory, Batavia, IL 60510-0500*<sup>3</sup>*Department of Astronomy & Astrophysics,**Enrico Fermi Institute, The University of Chicago, Chicago, IL 60637-1433***ABSTRACT**

Within the standard models of particle physics and cosmology we have calculated the big-bang prediction for the primordial abundance of  $^4\text{He}$  to a theoretical uncertainty of less than 0.1% ( $\delta Y_P < \pm 0.0002$ ), improving the current theoretical precision by a factor of 10. At this accuracy the uncertainty in the abundance is dominated by the experimental uncertainty in the neutron mean lifetime,  $\tau_n = 885.4 \pm 2.0$  sec. The following physical effects were included in the calculation: the zero and finite-temperature radiative, Coulomb and finite-nucleon-mass corrections to the weak rates; order- $\alpha$  quantum-electrodynamical correction to the plasma density, electron mass, and neutrino temperature; and incomplete neutrino decoupling. New results for the finite-temperature radiative correction and the QED plasma correction were used. In addition, we wrote a new and independent nucleosynthesis code designed to control numerical errors to be less than 0.1%. Our predictions for the  $^4\text{He}$  abundance are presented in the form of an accurate fitting formula. Summarizing our work in one number,  $Y_P(\eta = 5 \times 10^{-10}) = 0.2462 \pm 0.0004$  (expt)  $\pm < 0.0002$  (theory). Further, the baryon density inferred from the Burles-Tytler determination of the primordial D abundance,  $\Omega_B h^2 = 0.019 \pm 0.001$ , leads to the prediction:  $Y_P = 0.2464 \pm 0.0005$  (D/H)  $\pm < 0.0002$  (theory)  $\pm 0.0005$  (expt). This “prediction” and an accurate measurement of the primeval  $^4\text{He}$  abundance will allow an important consistency test of primordial nucleosynthesis.

# 1 Introduction

Big-bang nucleosynthesis (BBN) is one of the observational pillars of the standard cosmology. Further, it has the potential to be a precision probe of the early universe and fundamental physics [1, 2, 3]. Observations of light-element abundances have improved dramatically over the past few years, and the current and planned precision measurements of D,  $^4\text{He}$ ,  $^3\text{He}$  and  $^7\text{Li}$ , should allow a precise (10% or better) determination of the baryon density and consistency check of BBN, but only if the theoretical predictions of the light element abundances are as good as the observations. In particular, a measurement of the primeval D abundance pins down the baryon density, and in turn makes predictions for the other three abundances. Because the subsequent evolution of the  $^4\text{He}$  abundance is simple - stars make  $^4\text{He}$ - and measurements have the potential of determining  $Y_P$  to three significant figures [4, 5, 6, 7, 8, 9, 10],  $^4\text{He}$  can provide an important consistency check of BBN. Furthermore, an independent determination of the baryon density from cosmic microwave background anisotropies will soon test the consistency of the standard model of cosmology. Finally, the combination of accurate observations and theory can be used to test physics beyond the standard model of particle physics [1, 11], e.g., by imposing a strict limit on the number of light neutrino species [12, 13, 14]. Cosmology is entering a high precision age, and this motivates high-precision BBN predictions.

Over the years, theoretical study of  $^4\text{He}$  synthesis has been intense, with the following effects being considered: Coulomb and radiative corrections to the weak rates [15, 16, 17, 18, 19, 20], BBN code numerical errors [18], nuclear reaction rate uncertainties [21, 22], finite-temperature QED plasma corrections [15, 23], the effect of finite-nucleon mass [24, 25, 26], and incomplete neutrino decoupling [15, 27]. However, the corrections have been incorporated in a patchwork fashion and a recent informal poll of BBN codes indicated a spread of 1 % in the predicted value of the  $^4\text{He}$  abundance for fixed  $\eta$  and  $\tau_n$ .

The goal of this work was a calculation of the primordial abundance of  $^4\text{He}$ , within the standard models of particle physics and cosmology, accurate enough so that its uncertainty is dominated by the experimental uncertainty in the neutron mean lifetime<sup>1</sup>,  $\tau_n = 885.4 \pm 2.0 \text{ sec}$  [28, 29, 30]. Because  $\tau_n$  is so accurately known ( $\delta\tau_n/\tau_n = 0.23\%$ ), it is used to normalize all of the weak rates that interconvert neutrons and protons:  $ep \leftrightarrow \nu n$ ,  $e^+n \leftrightarrow \bar{\nu}p$  and  $n \leftrightarrow pe\bar{\nu}$ . The baryon-number fraction of  $^4\text{He}$  produced ( $\equiv Y_P$ ) depends sensitively on the weak rates because they determine the neutron-to-proton ratio  $n/p$  before nucleosynthesis, and essentially all of the neutrons around at the onset of nucleosynthesis go into forming  $^4\text{He}$ . We have determined the effect on  $Y_P$  by perturbing the weak rates in the standard code [31],

$$\frac{\delta Y_P}{Y_P} \simeq -0.8 \frac{\delta \Gamma}{\Gamma}. \quad (1)$$

Since the weak rates scale as  $1/\tau_n$ , this estimate implies that  $\delta\tau_n$  introduces an uncertainty in  $Y_P$  of 0.18%. We use this uncertainty to set our goal for all theoretical uncertainty.

---

<sup>1</sup>The Particle Data Group currently recommends  $\tau_n = 887 \pm 2 \text{ sec}$  [28]. A recent measurement using ultracold neutrons indicates a slightly lower value,  $\tau_n = 885.4 \pm 0.9 \text{ (stat)} \pm 0.4 \text{ (sys)} \text{ sec}$  [29]. For our central value we use 885.4 sec and for the uncertainty we use  $\pm 2 \text{ sec}$ .

To meet our goal we need to calculate the weak rates to precision of better than 0.23%. Another source of errors in  $Y_P$  come from thermodynamics, i.e., the energy density  $\rho$ , the pressure  $P$  and the neutrino temperature  $T_\nu$ . To determine how accurately we need to know thermodynamic quantities, we can estimate the change in  $Y_P$  due to a change in a thermodynamic quantity, e.g.,  $\rho$ . Again, using the standard code, we find

$$\frac{\delta Y_P}{Y_P} \simeq 0.4 \frac{\delta \rho}{\rho}, \quad (2)$$

This indicates that we should calculate thermodynamic quantities to better than 0.45%.

When calculating  $Y_P$  to this precision, several factors must be considered:

1. Weak rate and thermodynamics numerics: most quantities to be calculated involve integrations that must be done numerically.
2. ODE integration numerics: nucleosynthesis codes contain finite stepsize errors.
3. Nuclear reaction rates: errors originate from experimental uncertainties in the nuclear reaction data, as well as from neglecting nuclear reactions important to BBN.
4. Weak-rate physics: there are several small physical effects that must be calculated, including Coulomb, zero and finite-temperature radiative corrections, and the effect of finite-nucleon mass.
5. Thermodynamics physics: for temperatures much greater than the electron mass, there are order- $\alpha$  quantum electrodynamic corrections to the equation of state of the plasma.
6. Incomplete neutrino decoupling: neutrinos share partially in the entropy release when  $e^\pm$  pairs annihilate.

Items 1, 2 and 3 are addressed in the next Section; item 4 is addressed in Sec. 3. Items 5 and 6 are taken up in Sec. 4, and a summary of our results is given in the final section.

We mention that we have not considered the  $\mathcal{O}(\alpha^{3/2})$  collective plasma effects due to the presence of the copious numbers of  $e^\pm$  pairs at the time of BBN, because they are safely below our theoretical error budget of 0.1% for  $Y_P$ . These effects, all of relative size 0.1% and calculated in Ref. [32], are: the enhancement of nuclear reaction rates due to Debye screening of nuclear charge; the contribution of longitudinal plasmon modes ( $k \lesssim \omega_p \sim 4\pi n_{e^\pm}/T$ ) to the energy density and pressure; the (negative) contribution to the energy density and pressure of the electromagnetic interaction of  $e^\pm$  pairs; and the reduction of the energy and pressure of photons due to plasma effects on low frequency photons ( $k \lesssim \omega_p$ ). Finally, while we have tried to be exhaustive and very careful in our analysis, we cannot rule out systematic theoretical error: that is, the possibility that we have neglected some microphysical effect as important as those we have included.

## 2 Numerics

## 2.1 BBN Code

We have written a new nucleosynthesis code that is independent of the standard (Kawano) code [31]. The heart of any nucleosynthesis code is the set of ordinary differential equations that govern the evolution of the abundances of the light elements (see, e.g., Ref. [33, 34]). Our code tracks protons, neutrons, D, T,  $^3\text{He}$ ,  $^4\text{He}$ ,  $^6\text{Li}$ ,  $^7\text{Li}$  and  $^7\text{Be}$ . The baryon-number fraction of element  $i$  is given by<sup>2</sup>

$$X_i = \frac{A_i n_i}{n_B} = \frac{A_i (n_i/n_H)}{1 + \sum_i A_i (n_i/n_H)}, \quad (3)$$

where  $A_i$  is the element's atomic number,  $n_i$  it's number density, and  $n_B$  is the baryon-number density. (Note, by convention  $Y_P$  is used to denote  $X_4$ ). Nuclear reaction rates govern the evolution of the elemental abundances. Conservation of baryon number provides the constraint:

$$\sum_i X_i = 1.000. \quad (4)$$

We take for our initial temperature,  $T_i = 10$  MeV, and for our initial abundances, the nuclear statistical equilibrium (NSE) values:

$$X_A = g_A \left[ \zeta(3)^{A-1} \pi^{(1-A)/2} 2^{(3A-5)/2} \right] A^{5/2} \left( \frac{T}{m_N} \right)^{3(A-1)/2} \eta^{A-1} X_p^Z X_n^{A-Z} e^{B_A/T} \quad (5)$$

where  $A$  is the atomic number,  $m_N \simeq 940$  MeV is the nuclear mass,  $\eta$  is the baryon-to-photon ratio,  $B_A$  is the binding energy of species  $A$ , and  $\zeta(3) \simeq 1.20206$ . At temperatures greater than about 1 MeV, the nuclear rates are sufficiently high to cause the abundances to rapidly assume their NSE values. ( As discussed in Ref [35], the final abundances are very insensitive to the assumed initial abundances). If we make the well-justified assumption that the elements are always in kinetic equilibrium, then the rate coefficients depend only on  $\eta$  and  $T$ . This implies the important and well known conclusion that the predictions of nucleosynthesis are a function of only one parameter,  $\eta$ , which is equivalent to  $n_B$  since  $T_\gamma = 2.7277 \pm 0.002$  K is so well known.

Several important quantities enter into the evolution equations: weak rates, thermodynamic quantities and nuclear reaction rates. For the weak rates, we define the total conversion rates (per

---

<sup>2</sup>Baryon-number fraction and baryon-mass fraction differ by order 1% due to nuclear binding energy. Because nuclear reactions change the total mass in baryons, the mass fraction of species  $A_i$  ( $\equiv X_i^{\text{mass}}$ ) can change even if the number of species  $A_i$  does not. The mass fraction of species  $A_i$  is

$$X_i^{\text{mass}} = \frac{n_i m_i}{\sum_j n_j m_j} = \frac{n_i}{n_H} \frac{m_i}{m_H} \frac{1}{1 + \sum_j (n_j/n_H) (m_j/m_H)},$$

where  $m_i$  is the mass of species  $i$ : e.g.,  $m_4 = 4.002602$  amu and  $m_H = 1.00783$  amu. For  $Y_P = 0.25$  and the primordial mix of elements  $X_4^{\text{mass}} = 0.24866$ . Similarly, the relationship between the baryon mass density and  $\eta$  depends on elemental composition. For the primordial mix with  $Y_P = 0.25$ ,

$$\Omega_B h^2 = 3.66 \times 10^7 \eta,$$

with  $T_\gamma = 2.7277$  K. Assuming a mass of 1 amu per nucleon, the prefactor is  $3.639 \times 10^7$ , and for solar abundance, the prefactor is  $3.66043 \times 10^7$ .

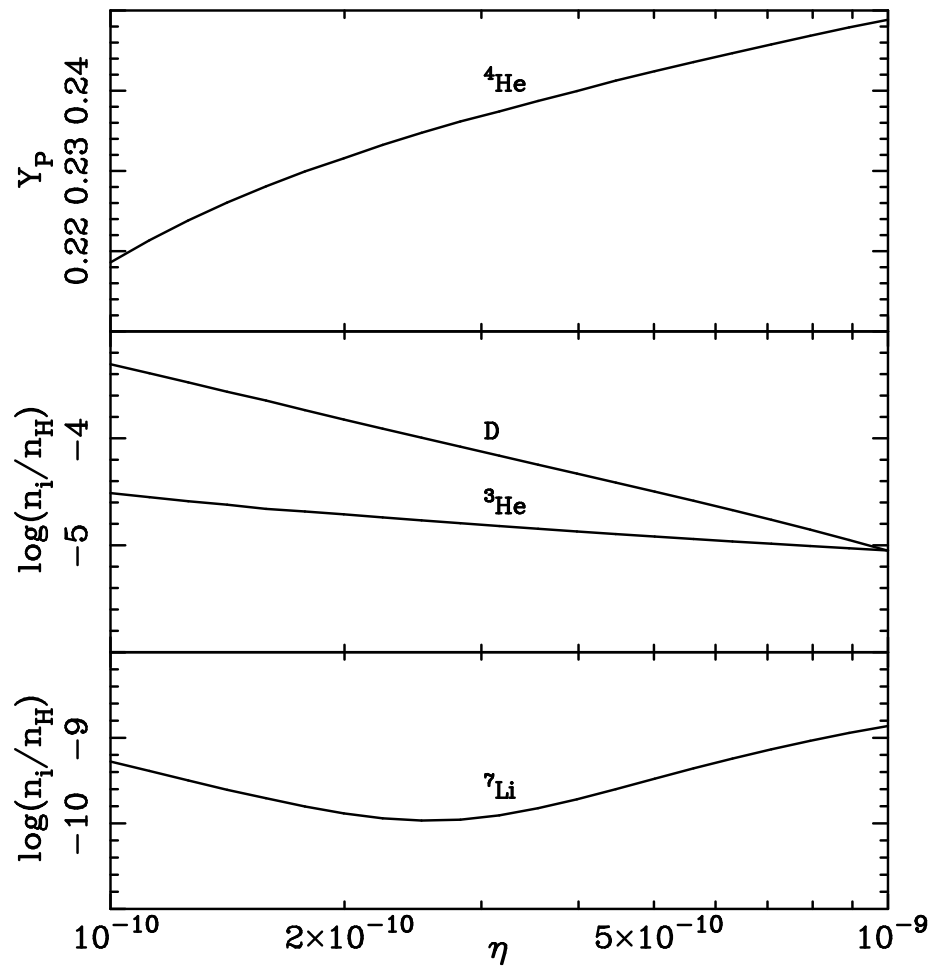


Figure 1: Baseline predictions: element abundances predicted by our BBN code.

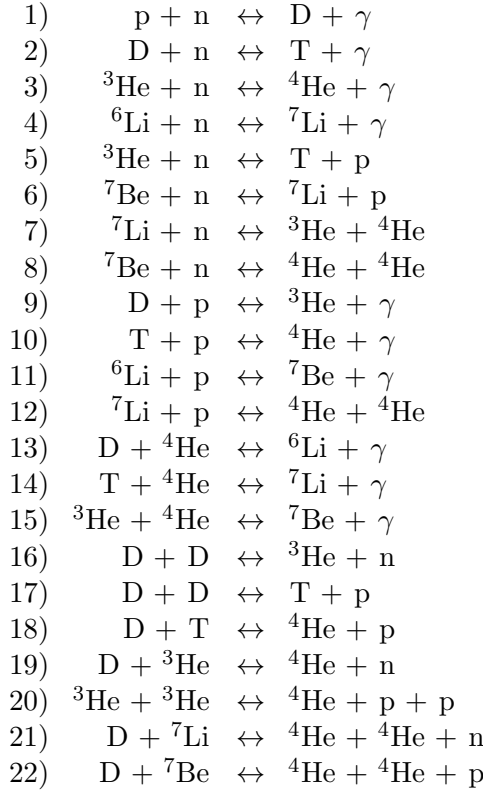


Table 1: Reactions used in our code.

neutron or proton):

$$\begin{aligned}\Gamma_{n \rightarrow p} &\equiv \Gamma_{e^+ n \rightarrow \bar{\nu} p} + \Gamma_{\nu n \rightarrow e p} + \Gamma_{n \rightarrow p e \bar{\nu}}, \\ \Gamma_{p \rightarrow n} &\equiv \Gamma_{e p \rightarrow \nu n} + \Gamma_{\bar{\nu} p \rightarrow e^+ n} + \Gamma_{p e \bar{\nu} \rightarrow n}.\end{aligned}\quad (6)$$

Simple expressions for these rates may be obtained assuming no radiative corrections and infinite nucleon mass. The thermodynamic quantities that must be calculated are  $\rho(T)$ ,  $T_\nu(T)$ ,  $\rho_B(T)$  and the differential time-temperature relation  $dt/dT$ .

Our BBN code is independent from the standard code, with one exception: It uses the same nuclear-rate data (with the exception of the weak rates). The nuclear-reaction network corresponds to the smallest one offered by the standard code, which contains the reactions listed in Table 1. Although this network is much smaller than the largest offered in the standard code, we have verified that the effect on  $Y_P$  of neglecting these additional reactions is less than  $10^{-4}$ . The light-element abundances predicted by our code are shown in Fig. 1.

## 2.2 Numerical Accuracy of the BBN Codes

Because the differential equations governing the light-element abundances are stiff, an implicit integrator was used to evolve them. Instead of specifying explicit time steps, as in the standard code, the desired final accuracies are specified as parameters of our code's integrator. The temperature

steps are then determined adaptively. Integrator accuracy parameters are chosen to be small enough so that stepsize errors were much smaller than the allowed error in  $Y_P$ .

To calculate the weak rates and thermodynamic quantities accurately, we proceed as follows (see, e.g., Ref. [36]). Let  $I = \int_a^b f(x) dx$  for some function  $f(x)$ . Expressed as a first order ordinary differential equation,  $I = J(b)$  where  $dJ/dx = f(x)$ ,  $J(a) = 0$ . We solve this differential equation using a fourth order Runge-Kutta routine. Figure 2 demonstrates for a specific example that the actual numerical errors are as small as requested. All of the weak rates and thermodynamic quantities were calculated so that their numerical error contributions to the uncertainty in  $Y_P$  were acceptably small.

We compared the results of our code to the standard code, which dates back to the original version written in 1966 [33], was updated by Wagoner in 1973 [34, 37], and modernized and made user friendly by Kawano in 1988 [38]. Nuclear reaction rates were updated in 1993[21]. One must be careful when making comparisons. First one must consider the numerical accuracy of the standard code. In 1992 Kawano [31] estimated the accuracy of  $Y_P$  to be 6 %. In 1993, Kernan addressed this issue in more detail and reported finding a systematic numerical error in the standard code [18, 39],  $\delta Y_P = 0.0017$ , large enough to be very significant at our level of accuracy. Second, the standard code implements certain physics corrections, namely a correction put in by Wagoner to approximate the Coulomb correction by scaling all of the weak rates a factor, 0.98, independent of temperature.

The systematic numerical error discovered by Kernan was measured by comparing the predictions of the standard code at some (unspecified) integration stepsize to the predictions as the stepsize became very small; note, however, that the error using the default stepsize (in Ref. [31]) is four times larger. The “Kernan correction” is now routinely added to the results of the standard code. Needless to say, a simple additive numerical correction is not adequate because other codes exist; not all users of the standard code use the same stepsize; and the numerical error can be machine dependent.

For our comparisons we took out the Kernan and Coulomb corrections and then made the stepsizes small enough so that integration errors were negligible. The integration error for the standard stepsizes (with the two standard stepsize parameters equal to 0.3 and 0.6, respectively) was found to be  $\delta Y_P = 0.0073$ . With the standard code configured this way, we compared  $Y_P$  and  $n_2/n_H$  as a function of  $\eta$  in two scenarios. For the first, we used the standard weak-rate routines to calculate the weak rates. For the second we used our high-precision weak-rate routines to calculate the weak rates in the standard code. The results are shown in Fig. 3. The agreement is excellent: for  $Y_P$  the codes differ by less than 0.15% with our weak-rate routines and by less than 0.2% with the standard weak-rate routines. For D the codes agree to better than 0.75%.

This agreement gave us confidence that our code calculates  $Y_P$  accurately for the baseline case (without the physics corrections). Of course, the convergence of two independent codes is not proof that they converge on the correct value. We will assume that the two codes do indeed converge on the the correct answer, and because our code was designed, engineered and tested for an error budget, we will use its results and internal error budget as the baseline for further comparison. The internal error budget for our code was no greater than 0.1%.

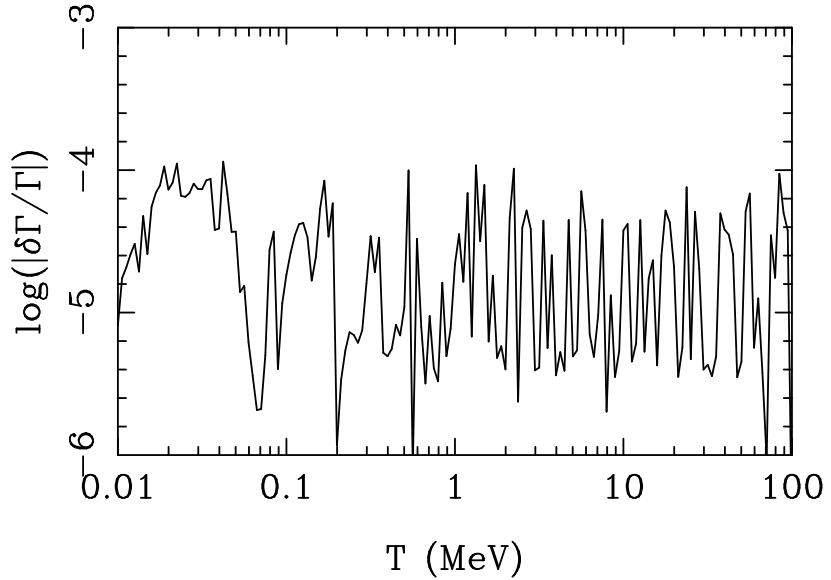


Figure 2: Actual numerical error in calculating  $\Gamma_{ep \rightarrow \nu n}$  for error parameter set at  $\delta\Gamma/\Gamma = 10^{-4}$ . The error is smaller than the specified accuracy ( $10^{-4}$ ) for all temperatures. Similar results were obtained for the other weak rates and thermodynamic quantities.

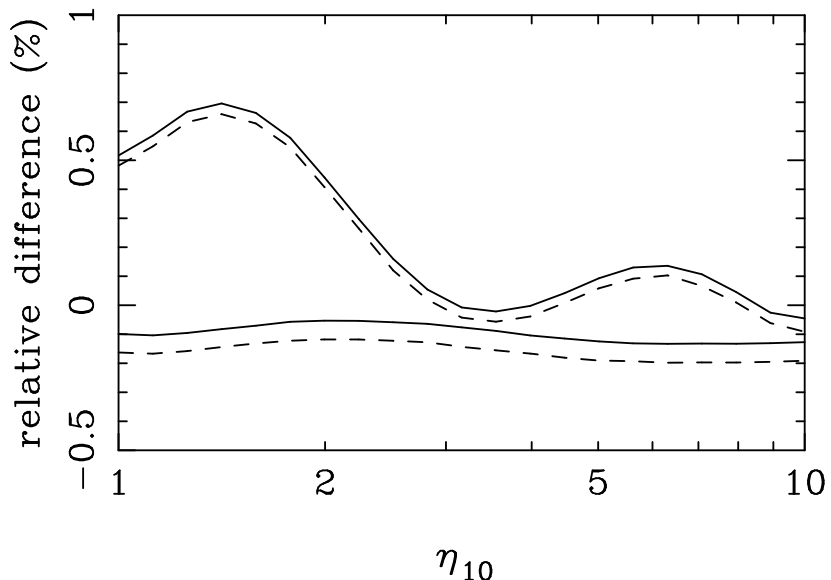


Figure 3: Comparison between the standard code and our code for  $^4\text{He}$  (lower curves) and D (upper curves). For the solid curves, our very accurate weak rates were inserted into the standard code. For the dashed curves, the standard code's weak rate routines were used. (Note:  $\eta_{10} \equiv \eta/10^{-10}$ ).

Reaction k	$\delta R_k/R_k$	$\delta Y_P/Y_P$ ( $\eta_{10} = 5.0$ )	$\delta Y_P/Y_P$ ( $\eta_{10} = 1.8$ )
$n \leftrightarrow p$	0.23%	0.17%	0.18%
$p(n, \gamma)d$	7%	0.04%	0.17%
$d(d, n)^3He$	10%	0.06%	0.07%
$d(d, p)T$	10%	0.05%	0.06%
Total Uncertainty		0.19%	0.27%

Table 2:  $1-\sigma$  experimental uncertainties and their effect on  $Y_P$ . All nuclear rates whose uncertainties significantly impact  $Y_P$  are shown. The weak-rate uncertainty of 0.23% is due to uncertainty in measurements of the neutron mean lifetime, and assumes that Coulomb, radiative and thermodynamic corrections to the weak rates are known to better accuracy than this. Note that for  $\eta = 5.0 \times 10^{-10}$ , the neutron mean lifetime dominates the error budget. The bottom row indicates the RMS total uncertainty in  $Y_P$  for these two values of  $\eta$ .

### 2.3 Nuclear Rate Uncertainties

The primordial  ${}^4He$  abundance is sensitive to nuclear reactions other than the weak rates. Several studies of the uncertainties in theoretical abundances due to nuclear rate uncertainties have been performed [1, 21, 39, 40, 41, 42]. Here we will use the results and techniques of the recent work of Fiorentini, et al [22]. They use linear error propagation theory to quantify the effect of experimental uncertainties in the nuclear-reaction rates on the light element abundance uncertainties and their correlations,

$$\left(\frac{\delta Y_P}{Y_P}\right)^2 = \sum_k \lambda_k^2 \left(\frac{\delta R_k}{R_k}\right)^2, \quad (7)$$

where the sum  $k$  is over nuclear reactions,  $\delta R_k$  is the experimental uncertainty in the rate  $R_k$ , and  $\lambda_k$  is the logarithmic derivative

$$\lambda_k = \frac{\partial \log Y_P}{\partial \log R_k}. \quad (8)$$

Fiorentini, et al [22] calculate the logarithmic derivatives numerically, using the standard code, and take the experimental rate uncertainties from Smith, et al [21]. Contributions to the uncertainty in the  ${}^4He$  abundance arise almost entirely from four rates. Table 2.3 lists these rates and their relative experimental uncertainties. Figure 4 shows the resulting uncertainty in  $Y_P$ . For  $\eta \leq 2 \times 10^{-10}$ , the reaction  $p(n, \gamma)d$  dominates the error budget. Finally, a recent new analysis of the experimental uncertainties [43], indicates the uncertainties in the reactions  $d(d, n)p$  and  $d(d, p)T$  have been overestimated by about a factor of two, and that the precision of the reaction  $p(n, \gamma)d$  could be improved significantly. Thus it may well be the case that the uncertainty in  $\tau_n$  dominates the error budget for all  $\eta$ .

## 3 Weak Rates

The primordial  ${}^4He$  abundance is very sensitive to the weak rates that maintain the balance between neutrons and protons. To calculate  $Y_P$  to a precision of 0.12% the weak rates must be known to

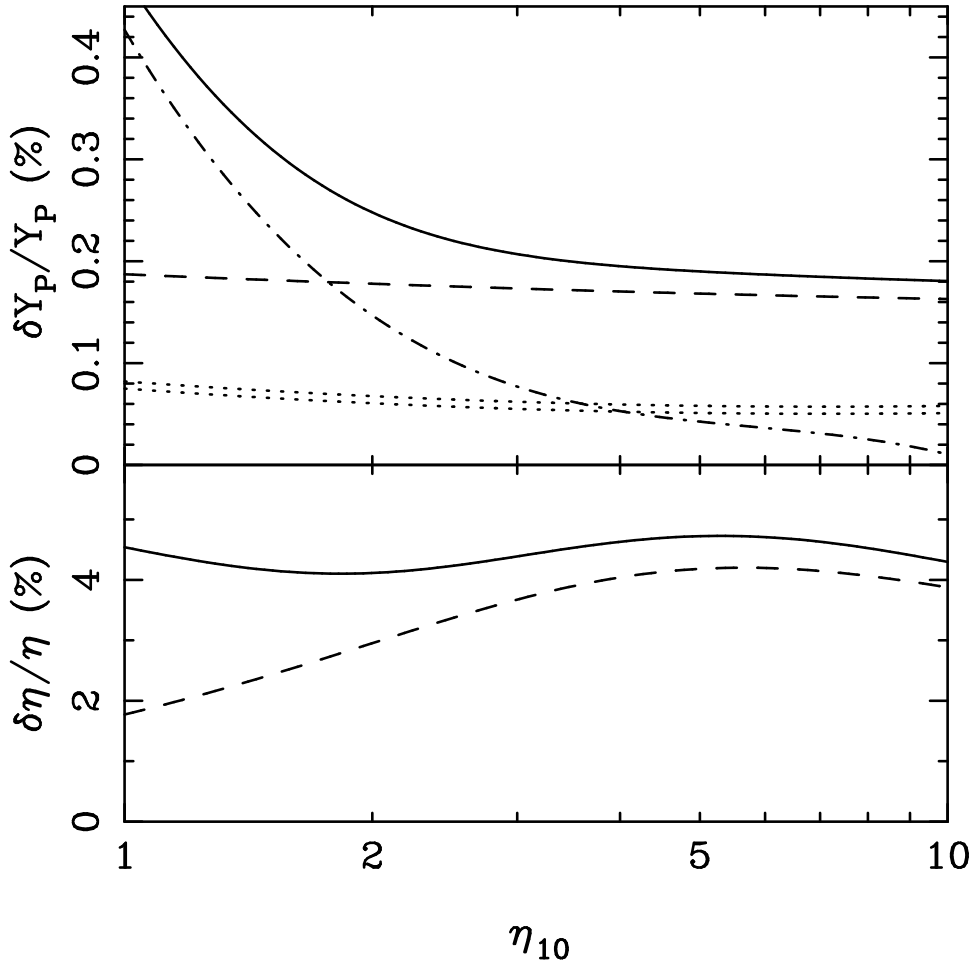


Figure 4: The top panel shows the uncertainty in  $Y_P$  due to experimental uncertainties in nuclear rates, as a function of  $\eta$ . The solid line shows the total uncertainty, while the other lines show each nuclear reaction separately. The dashed line is for  $n \leftrightarrow p$ , the dashed-dotted line is for  $p(n, \gamma)d$ , and the two dotted lines are for  $d(d, n)^3\text{He}$  and  $d(d, p)\text{T}$ . The bottom panel shows the uncertainty in  $\eta$  that would result from the above uncertainties in  $Y_P$ , when  $\eta$  is derived from a perfect measurement of the  ${}^4\text{He}$  abundance. The dashed line is for the weak rate uncertainties alone, while the solid line is for the total nuclear rate uncertainty. The factor of ten difference in the scales between the two panels is indicative of the fact that  $Y_P$  depends logarithmically upon  $\eta$ .

a precision of 0.15%. In addition to numerical issues discussed earlier, several physical effects are important at this level: zero-temperature radiative and Coulomb corrections, finite-nucleon mass correction, and finite-temperature radiative correction.

The expressions for the weak rates are derived starting with the tree-level (Born diagram) shown in Fig. 5. For purposes of illustration, we will consider the process  $e^- + p \rightarrow \nu_e + n$ . Without making any approximations the phase space integral for the conversion rate (per proton) can be simplified to a five-dimensional integral involving the matrix-element squared  $|\mathcal{M}|^2$  [26]

$$\Gamma_{ep \leftrightarrow \nu n} = \frac{1}{2^9 \pi^6 n_p} \int dp_e dp_p d \cos \theta_p d \cos \theta_\nu d \phi_\nu \times \frac{p_e^2 p_p^2 E_\nu}{E_e E_p E_n} \frac{1}{\mathcal{J}} |\mathcal{M}|^2 f_e f_p (1 - f_\nu) (1 - f_n), \quad (9)$$

$$\mathcal{J} = 1 + \frac{E_\nu}{E_n} \left( 1 - \frac{(\mathbf{p}_e + \mathbf{p}_p) \cdot \mathbf{p}_\nu}{E_\nu^2} \right), \quad (10)$$

where  $E_e$ ,  $E_p$ ,  $E_\nu$ , and  $E_n$  denote the energies of the respective particles and  $\mathcal{J}$  is the Jacobian introduced in integrating the energy part of the delta function, and  $|\mathcal{M}|^2$  is summed over initial and final state spins. The integration limits correspond to the kinematically allowed region in the five-variable phase space. An expression for  $E_\nu = p_\nu$  in terms of the integration variables  $p_e, p_p, \theta_p, \theta_\nu$ , and  $\phi_\nu$  is given by

$$\begin{aligned} p_\nu &= \frac{A^2 B + 2E \sqrt{A^4 - m_\nu^2(4E^2 - B^2)}}{4E^2 - B^2}, \\ A^2 &\equiv 2E_e E_p + m_\nu^2 - m_n^2 - m_e^2 - m_p^2 - 2p_e p_p \cos \theta_p, \\ B &\equiv 2 [p_e \cos \theta_\nu + p_p (\cos \theta_p \cos \theta_\nu + \sin \theta_p \sin \theta_\nu \cos \phi_\nu)]. \end{aligned} \quad (11)$$

where  $E = E_e + E_p$ . For more details, see Ref. [26].

This rate expression is challenging to evaluate for two reasons. First, the kinematically allowed region in the five-dimensional phase space is not simple. Second, the full matrix element is complex. Only if the nucleons are assumed to be infinitely massive, does the expression simplify:  $|\mathcal{M}|^2 \rightarrow 2^5 G_F^2 (1 + 3g_A^2) E_e E_p E_\nu E_n$ . In that limit, the sole kinematical constraint is  $E_p = E_\nu + Q$ , ( $Q = m_n - m_p = 1.293$ , MeV), and the rate expression becomes a one variable integration. Normalizing the rates to the zero-temperature free neutron decay rate,

$$\frac{1}{\tau_n} \equiv \Gamma_{n \rightarrow pe\nu}(T=0) = \frac{G_F^2 (1 + 3g_A^2) m_e^5}{2\pi^3} \lambda_0, \quad (12)$$

$$\lambda_0 = \int_1^q d\epsilon \epsilon (\epsilon - q)^2 (\epsilon^2 - 1)^{1/2} = 1.6333, \quad (13)$$

leads to the well known formula for the process  $ep \rightarrow \nu n$ :

$$\Gamma_{ep \rightarrow \nu n}^\infty = \frac{1}{\tau_n \lambda_0} \int_q^\infty \frac{\epsilon (\epsilon^2 - q^2)^{1/2}}{[1 + \exp(\epsilon z)] [1 + \exp((q - \epsilon) z_\nu)]}, \quad (14)$$

where  $T$  is the photon temperature,  $T_\nu$  is the neutrino temperature,  $\epsilon \equiv E_e/m_e$ ,  $q \equiv Q/m_e$ ,  $z \equiv m_e/T$ , and  $z_\nu \equiv m_e/T_\nu$ . Summing the  $n \rightarrow p$  and  $p \rightarrow n$  rates yields the standard weak-rate

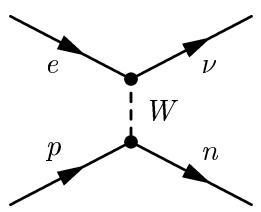


Figure 5: Tree level diagram for the process  $ep \rightarrow \nu n$ .

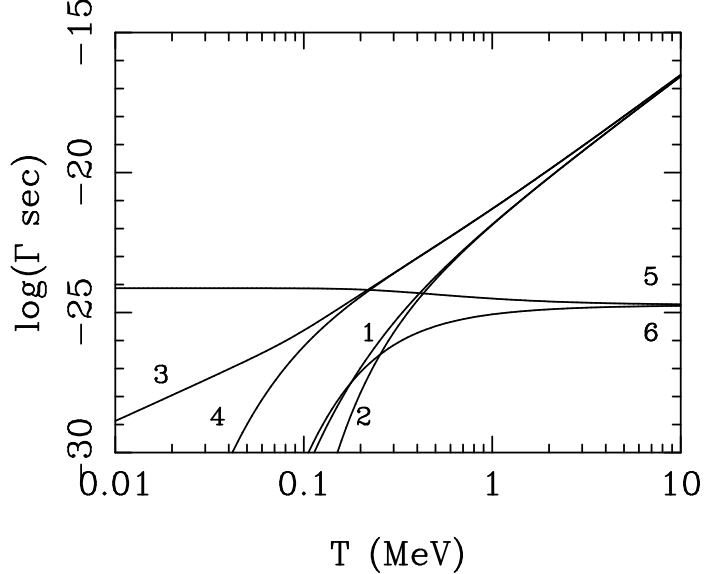


Figure 6: Weak rates as a function of temperature (Born diagram, infinite-nucleon-mass limit): (1)  $ep \rightarrow \nu n$ , (2)  $\nu p \rightarrow en$ , (3)  $en \rightarrow \nu p$ , (4)  $\nu n \rightarrow ep$ , (5)  $n \rightarrow pe\nu$ , (6)  $pe\nu \rightarrow n$ . Note, freeze-out of the  $n/p$  ratio occurs at  $T_F \simeq 0.8$  MeV and  ${}^4\text{He}$  synthesis begins at  $T \simeq 0.1$  MeV.

expressions [44]

$$\begin{aligned}\Gamma_{n \rightarrow p} &= \frac{1}{\tau_n \lambda_0} \left( - \int_{-\infty}^{-1} + \int_1^{\infty} \right) d\epsilon \frac{\epsilon(\epsilon - q)^2 \sqrt{\epsilon^2 - 1}}{(1 + e^{-\epsilon z})(1 + e^{(q-\epsilon)z_\nu})}, \\ \Gamma_{p \rightarrow n} &= \frac{1}{\tau_n \lambda_0} \left( - \int_{-\infty}^{-1} + \int_1^{\infty} \right) d\epsilon \frac{\epsilon(\epsilon - q)^2 \sqrt{\epsilon^2 - 1}}{(1 + e^{\epsilon z})(1 + e^{(\epsilon-q)z_\nu})}.\end{aligned}\quad (15)$$

The six individual rates are plotted as a function of temperature in Fig. 6.

### 3.1 Zero-Temperature Coulomb and Radiative Corrections

To order  $\alpha$ , the weak rates with zero-temperature Coulomb and radiative corrections are given by the sum of the interference between the Born diagram (Fig. 5) and the diagrams in Fig. 7.

It is conventional to separate the corrections into a Coulomb part proportional to nuclear charge  $Ze$  and a radiative part proportional to  $e$ . Since  $Z = 1$  here, this separation is arbitrary. Dicus et al calculated the Coulomb and zero-temperature radiative corrections to the weak rates in 1982 [15]. Summarizing their results we obtain the following prescription for correcting the rates. First, perform the zero-temperature radiative corrections by multiplying the integrands of all of the rates by the factor,

$$\left[ 1 + \frac{\alpha}{2\pi} C(\beta, y) \right], \quad (16)$$

where

$$\begin{aligned}C(\beta, y) &= 40 + 4(R-1) \left( \frac{y}{3\epsilon} - \frac{3}{2} + \ln 2y \right) + R \left( 2(1 + \beta^2) + \frac{y^2}{6\epsilon^2} - 4\beta R \right) \\ &\quad - 4(2 + 11\beta + 25\beta^2 + 25\beta^3 + 30\beta^4 + 20\beta^5 + 8\beta^6)/(1 + \beta)^6,\end{aligned}\quad (17)$$

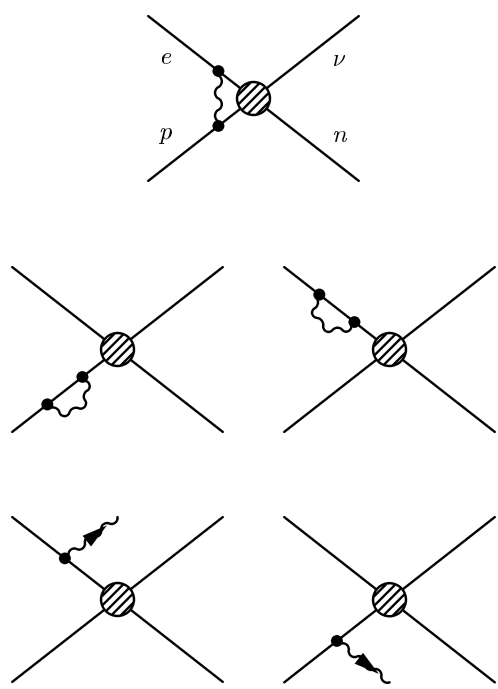


Figure 7: Zero-temperature corrections to the process  $ep \rightarrow \nu n$ . The center blob is the charged-current, weak-interaction vertex.

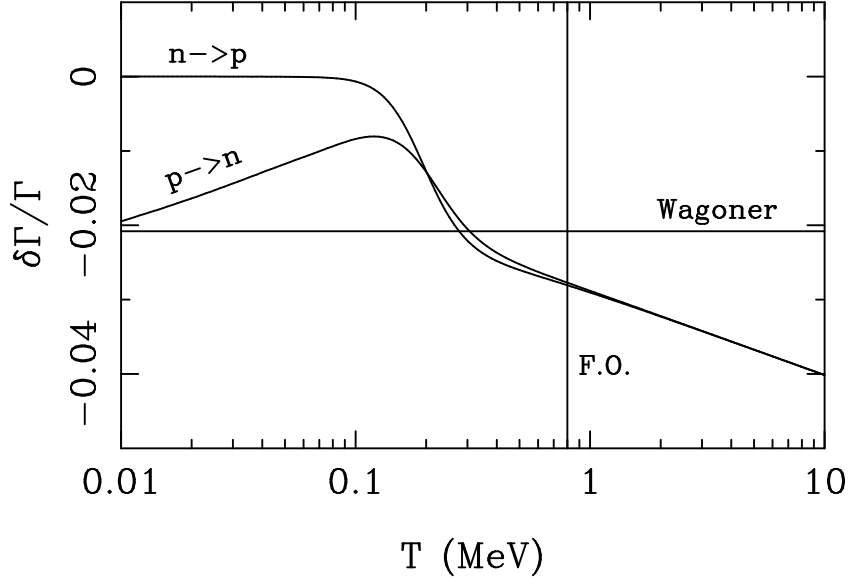


Figure 8: Zero-temperature radiative and Coulomb corrections to the  $n \leftrightarrow p$  rates. The horizontal line is Wagoner's approximation to the Coulomb correction. The vertical line is at freeze-out.

$\beta$  is the electron's velocity and  $R = \tanh \beta^{-1}/\beta$ . Next apply the Coulomb correction by multiplying the integrand of the rates for  $n \leftrightarrow pe\nu$  and  $ep \leftrightarrow \nu n$  by the non-relativistic Fermi factor,

$$F(\beta) = \frac{2\pi\alpha/\beta}{1 - e^{-2\pi\alpha/\beta}}. \quad (18)$$

The error from using the non-relativistic Fermi function is of order 2% of the Coulomb effect itself [45], and so the approximation is fine. Finally,  $\lambda_0$  must be corrected for Coulomb and zero-temperature radiative effects by multiplying it's integrand by  $[1 + \frac{\alpha}{2\pi}C(\beta, y)] F(\beta)$ . Doing this increases  $\lambda_0$  by 7.15%, to 1.7501.

Figure 8 shows the combined zero-temperature corrections. Note that the corrections are less than or equal to zero for both rates for all temperatures: decreased weak rates imply earlier  $n/p$  freeze-out and an increase in  $Y_P$ . Our code calculates the zero-temperature corrections to the weak rates by modifying the integrands of the rate expressions as described above, and by using the corrected  $\lambda_0$ . The zero-temperature corrections yield a change,  $\delta Y_P/Y_P = 1.28\%$  which is insensitive to the value of  $\eta$  over the range  $10^{-10} \leq \eta \leq 10^{-9}$ . This result is in agreement with Ref. [15].

Wagoner approximated the Coulomb correction by reducing both the  $n \rightarrow n$  and  $p \rightarrow n$  rates by 2%. This correction, shown by the horizontal line, is close to the high temperature asymptotic Coulomb correction of  $-2.16\%$ . However,  $n/p$  continues to decrease slowly for temperatures lower than freeze-out, where Wagoner's approximation breaks down. The fact that the real corrections are less negative in this regime means that the change in  $Y_P$  from the Coulomb correction will be less positive than one would estimate from Wagoner's approximation. Adding in the zero-temperature radiative corrections brings the total zero-temperature change in  $Y_P$  closer to what would be found using Wagoner's approximation to the Coulomb correction. Table 3.1 shows

Correction	$\delta Y_P / Y_P$
Coulomb	1.04%
T=0 Radiative	0.24%
Combined	1.28%
Wagoner's approximation	1.56%

Table 3: Zero-temperature corrections to  $Y_P$ , compared with change in  $Y_P$  from Wagoner's approximation of the Coulomb correction. These corrections are insensitive to  $\eta$  for  $10^{-10} \leq \eta \leq 10^{-9}$ .

$\delta Y_P / Y_P$  for the Coulomb and zero-temperature radiatively separately and summed, compared to  $\delta Y_P / Y_P$  from Wagoner's approximation. Note in particular that the difference between Wagoner's approximation and the zero-temperature correction is 0.28%, which is significant at the 0.1% level.

### 3.2 Finite-Nucleon Mass Correction

Recall that the standard rate expressions, Eqn.(14), assume infinitely massive nucleons. We have calculated the weak rates without this assumption by numerically integrating the five-dimensional rate integral, Eqn.(9), using the Monte Carlo method [26]. Figure 9 shows the finite-mass corrections to the  $n \leftrightarrow p$  rates. Using the individual rate corrections we found the corrections to the summed  $n \leftrightarrow p$  rates,

$$\frac{\delta \Gamma_{n \rightarrow p}}{\Gamma_{n \rightarrow p}} \equiv \frac{\Gamma_{n \rightarrow p} - \Gamma_{n \rightarrow p}^\infty}{\Gamma_{n \rightarrow p}^\infty} \quad (19)$$

$$\frac{\delta \Gamma_{p \rightarrow n}}{\Gamma_{p \rightarrow n}} \equiv \frac{\Gamma_{p \rightarrow n} - \Gamma_{p \rightarrow n}^\infty}{\Gamma_{p \rightarrow n}^\infty}, \quad (20)$$

where  $\Gamma^\infty$  is the rate in the infinite-mass approximation, and  $\Gamma$  is the unapproximated rate. Our corrections are accurate to within a few percent [26]. We incorporated the finite-mass corrections into our code by modifying the  $n \leftrightarrow p$  rates at each temperature by the correction shown in Fig. 9. The resulting correction to  $Y_P$  was found to be  $\delta Y_P / Y_P = 0.50\%$ , valid for  $10^{-10} \leq \eta \leq 10^{-9}$ .

### 3.3 Finite-Temperature Radiative Correction

Finite-temperature modifications to the weak rates arise from several sources:

1. the  $(1 \pm f)$  quantum statistical factors in the integration over phase space
2. a shift in the electron mass
3. a change in the neutrino-to-photon temperature ratio
4. a correction to the photon and fermion propagators
5. the square of the sum of diagrams for processes that involve photons from the plasma (absorption and stimulated emission); see Fig. 10.
6. finite-temperature wave-function renormalization

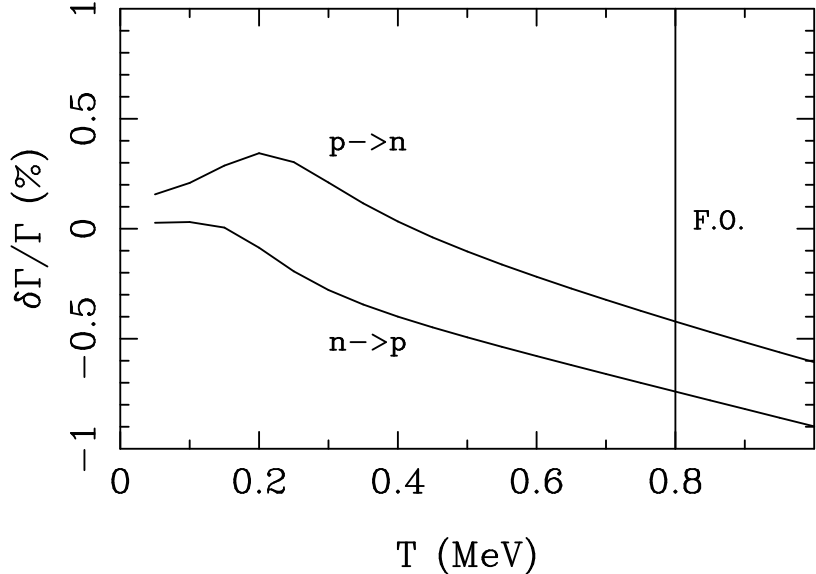


Figure 9: Finite-nucleon-mass correction to the  $n \leftrightarrow p$  rates. The freeze-out temperature,  $T_F \simeq 0.8$  MeV, is indicated with a vertical line.

Item 1 is included in our definition of the Coulomb correction. We shall define items 2 and 3 to be part of the thermodynamics effects, considered later. Therefore, the finite-temperature radiative correction to the weak rates involves items 4, 5 and 6.

Dicus, et al [15], and Cambier, Primack and Sher [46] calculated the finite-temperature radiative corrections to the weak rates. Neither of these papers correctly handle the finite-temperature wave-function renormalization. In fact, finite-temperature wave-function renormalization is still an open issue. The difficulty lies in the fact that finite temperature spoils Lorentz covariance through the existence of a preferred, thermal frame (in this frame the phase-space distributions are the Bose-Einstein or Fermi-Dirac distributions). The usual methods for obtaining the wave-function renormalization rely on Lorentz covariance, so that the appropriate generalization to the finite-temperature case is not clear. Donoghue and Holstein [16, 17] start by assuming a finite-temperature spinor field – with creation and annihilation operators obeying the standard anti-commutation relations – that satisfies the nonlinear Dirac equation. They write the propagator in terms of these finite-temperature scalars, obtaining a finite-temperature wave-function renormalization that is a multiplicative factor. Sawyer [19], and Esposito, et al [47], start by identifying particle states with poles of the propagator, without reference to the finite-temperature field. They assume that the poles are only perturbatively shifted from their zero-temperature values. They then identify the finite-temperature wave-function renormalization with the residue of the propagator at the new pole. The result is a finite-temperature wave-function renormalization that contains additional, non multiplicative terms, so that the results of the two alternative approaches are different (as pointed out by Chapman [20]). Furthermore, the results of the Sawyer differ from Esposito, et al [47], even though they follow similar approaches. The differences change the rates for some processes. *However, for the case of the weak rates, the three different finite-temperature wave-function renormalization results give the same contribution to the weak rates.* For convenience, we

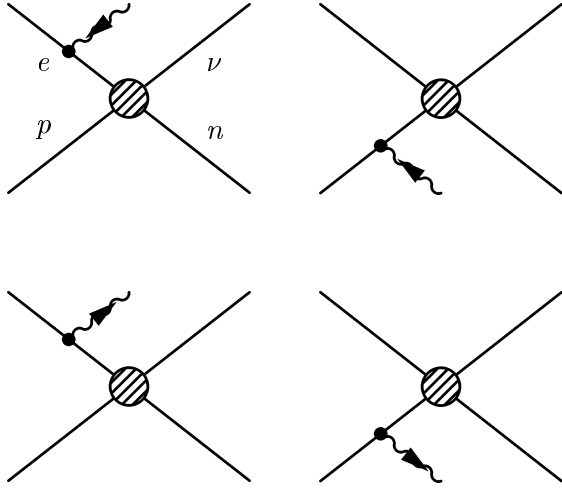


Figure 10: Finite-temperature corrections to the weak rates, i.e., corrections involving photons from the plasma. The bottom two diagrams represent stimulated emission.

used the formalism of Sawyer. The correction to the  $en \rightarrow \nu p$  is given as

$$\delta\Gamma = \frac{e^2 T^4}{2^4 \pi^5} G_F^2 (1 + 3g_A^2) \times \int_0^\infty \int_x^\infty du dk_v p_u N_+(u) [N_-(k_v) W_\gamma(u, k_v) + N_+(v) W_r(u, k_v)], \quad (21)$$

where  $x = m/T$ ,  $p_u = \sqrt{u^2 - x^2}$ ,  $v = \sqrt{k_v^2 + x^2}$ ,  $N_\pm(u) = 1/(e^u \pm 1)$ ,

$$W_\gamma(u, k_v) = \left[ \left( \frac{k_v}{2p_u} + \frac{u^2}{k_v p_u} \ln \frac{u + p_u}{u - p_u} - \frac{2u}{k_v} \right) [H(u + k_v) + H(u - k_v) - 2H(u)] + \left[ \frac{u}{p_u} \ln \frac{u + p_u}{u - p_u} - 2 \right] [H(u + k_v) - H(u - k_v)] \right] \quad (22)$$

$$W_r(u, k_v) = \frac{k_v H(u)}{4p_u v} \left[ 2u \ln \frac{p_u + k_v}{p_u - k_v} + v \ln \frac{m^4 - (uv - p_u k_v)}{m^4 - (uv + p_u k_v)} - \frac{4k_v p_u u}{p_u^2 - k_v^2} \right] \quad (23)$$

and

$$H(w) = \nu^2 N(-\nu) \Theta(\nu), \quad (24)$$

$$\nu = (w + q) \quad (25)$$

with  $q = Q/T$ . The term proportional to  $W_r$  is due to finite-temperature wave function renormalization. To find the correction to the other weak rates, make the substitutions shown in Table 4.

We calculated the finite-temperature radiative corrections to each of the weak rates. The correction to the summed  $n \leftrightarrow p$  rates, which match Sawyer's results, are shown in Fig. 11. The correction formulas are complicated enough to preclude direct incorporation into our BBN code. Therefore we implemented these corrections as temperature-dependent fits within the BBN code. The resulting change in  $Y_P$ ,  $\delta Y_P/Y_P = 0.12\%$ , was found to be insensitive to  $\eta$  in the range  $10^{-10} \leq \eta \leq 10^{-9}$ . Sawyer claims a change of  $+0.02\%$ , while Chapman claims a change of  $+0.01\%$ .

process	lower u-limit	upper u-limit	e-Fermi 1	e-Fermi 2	$\nu$	$N(\pm\nu)$
$en \rightarrow \nu p$	$x$	$\infty$	$N(u)$	$N(v)$	$w + q$	$-\nu$
$ep \rightarrow \nu n$	$q$	$\infty$	$N(u)$	$N(v)$	$w - q$	$-\nu$
$\nu n \rightarrow ep$	$q$	$\infty$	$N(-u)$	$N(-v)$	$w - q$	$+\nu$
$\nu p \rightarrow en$	$x$	$\infty$	$N(-u)$	$N(-v)$	$w + q$	$+\nu$
$n \rightarrow pe\nu$	$x$	$q$	$N(-u)$	$N(-v)$	$-w + q$	$-\nu$
$pe\nu \rightarrow n$	$x$	$q$	$N(u)$	$N(v)$	$-w + q$	$+\nu$

Table 4: Substitutions in Eqs. (21–25) for computing finite-temperature radiative corrections.

Both Sawyer and Chapman compute the change in the neutron fraction to estimate  $\delta Y_P/Y_P$ . To first order in the perturbation, the equations governing the evolution of the neutron fraction  $X_n$  and its perturbation  $\delta X_n$ , can be written

$$\begin{aligned} \frac{d X_n}{dT} &= \frac{dt}{dT} [-X_n \Gamma_{n \rightarrow p} + (1 - X_n) \Gamma_{p \rightarrow n}] \\ \frac{d \delta X_n}{dT} &= \frac{dt}{dT} \{ \Gamma_{n \rightarrow p} (\delta X_n + \gamma_n X_n) + \Gamma_{p \rightarrow n} [\gamma_p (1 - X_n) - \delta X_n] \}, \end{aligned} \quad (26)$$

where  $\gamma_n = \delta \Gamma_{n \rightarrow p} / \Gamma_{n \rightarrow p}$  and  $\gamma_p = \delta \Gamma_{p \rightarrow n} / \Gamma_{p \rightarrow n}$ . Then the change in  $Y_P$  is estimated as

$$\frac{\delta Y_P}{Y_P} \simeq \frac{\delta X_n}{X_n} \Big|_{\text{onset of BBN}} \simeq \frac{\delta X_n}{X_n} \Big|_{T=0}. \quad (27)$$

In order to have a direct comparison with the results of Sawyer and Chapman, we found  $\delta Y_P/Y_P$  using this method. The evolution of  $\delta X_n$  is shown in Fig. 12. Our results obtained from this approximation method confirm those using the BBN code, and differ from Sawyer and Chapman. However, all agree the change in  $Y_P$  is small.

## 4 Thermodynamics

Thermodynamic corrections refer to corrections to the density, pressure and neutrino-to-photon temperature ratio. There are two effects to consider: finite-temperature QED corrections to the equation of state of the electromagnetic plasma, and incomplete neutrino decoupling.

### 4.1 Finite-temperature QED Correction

The finite-temperature QED corrections encompass corrections to the density, neutrino temperature and electron mass. All of the these corrections follow from the finite-temperature QED modification to the equation of state of the electromagnetic plasma. These corrections were calculated by Heckler [23] and applied to cosmology and solar physics. We will follow his approach, correcting a few small errors.

The  ${}^4\text{He}$  abundance is sensitive to thermodynamic quantities in several ways. The energy density determines the expansion rate; changes in the expansion rate affect the freeze-out temperature, the abundance of free neutrons, and finally  $Y_P$ . The next two effects follow from corrections to the

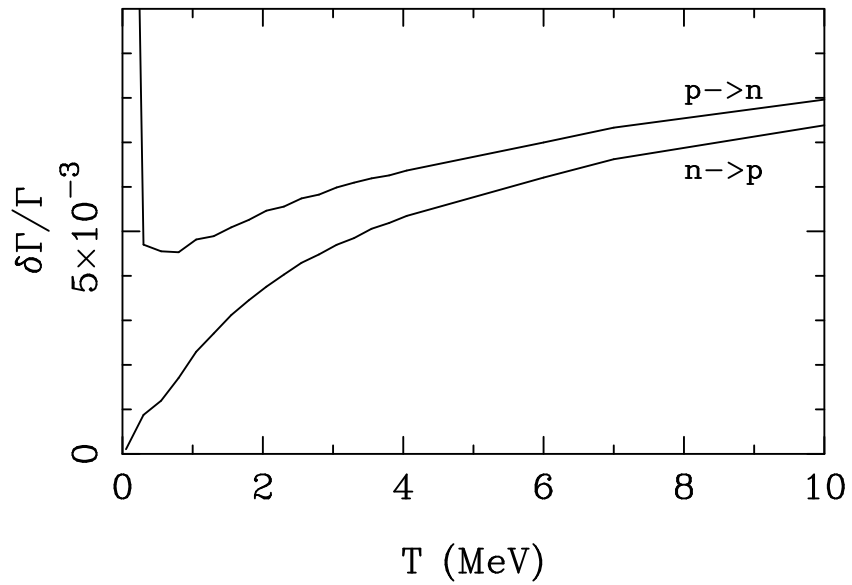


Figure 11: Finite-temperature radiative corrections to the  $n \leftrightarrow p$  rates. This plot is to be compared to Fig. 4 in Ref. [12].

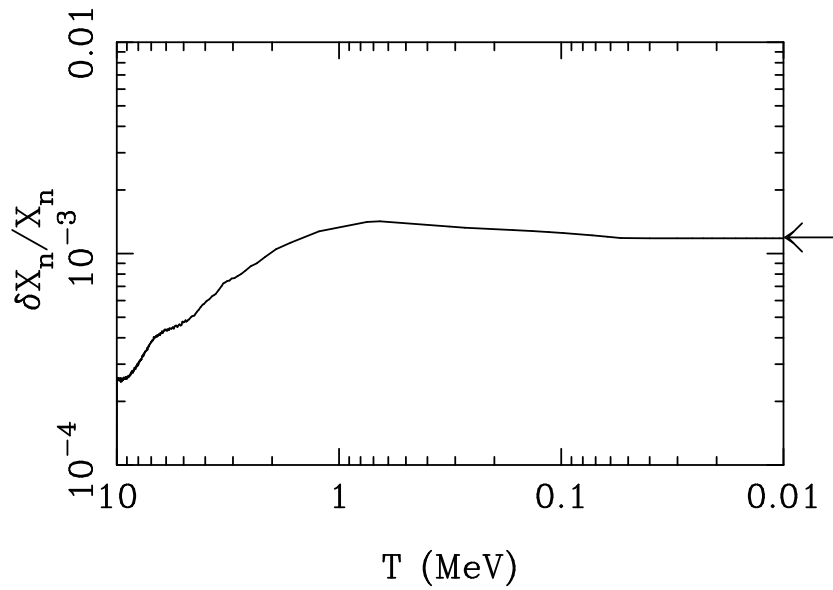


Figure 12: Temperature evolution of the estimated change in neutron fraction  $X_n$  due to finite-temperature radiative corrections. The solid line shows the results of integrating the perturbation equations; the low-temperature asymptotic solution gives the correction to  $Y_P$ ,  $\delta Y_P/Y_P = \delta X_n/X_n$ . The arrow indicates the final result of substituting the radiative corrections into our full code. The two methods agree very well.

electron mass. A change in the electron mass affects the weak rates directly, and indirectly, by changing the entropy of the electron-positron plasma at the time neutrinos decouple. Since this entropy is transferred to the photons when the  $e^\pm$  pairs disappear, this changes the neutrino-to-photon temperature ratio, and affects the weak rates, which are very sensitive to the neutrino temperature.

The finite-temperature QED correction to the equation of state can be expressed as a modification to the pressure of the pressure-weighted, effective number of effective degrees of freedom,

$$P(T) = P_0(T) + \delta P(T), \quad (28)$$

where  $\delta P(T)$  is the correction to the pressure and  $P_0(T) = (\pi^2/90) g_P T^4$  is the standard expression for the pressure. The change in pressure can be equated to a change in  $g_\rho$ ,  $\delta g_P = 90/(\pi^2 T^4) \delta P$ . The correction  $\delta P(T)$  can be expressed as an expansion in electron charge  $e \simeq 0.301$ :  $\delta P(T) = \sum_i \delta P_i(T)$ . The Feynman diagrams for the  $e^2$ -term and  $e^3$ -term are shown in Fig. 4.1. For vanishing chemical potential the  $e^2$  term is [48],

$$\begin{aligned} \delta P_2(T) = & -\frac{e^2 T^4}{6\pi^2} \int_x^\infty du \frac{\sqrt{u^2 - x^2}}{e^u + 1} \\ & -\frac{e^2 T^4}{8\pi^3} \int_x^\infty \int_x^\infty du dv p_u p_v N(u) N(v) \left( 4 + \frac{x^2}{p_u p_v} \ln \frac{u v + p_u p_v + x^2}{u v - p_u p_v + x^2} \right), \end{aligned} \quad (29)$$

where  $x \equiv m_e/T$ ,  $u \equiv E_u/T$ ,  $p_u \equiv \sqrt{u^2 - x^2}$  and  $N(u) = 1/(1 + e^u)$ . In the high-temperature limit  $T \gg m_e$ ,

$$\delta P_2(T) \simeq -\frac{5e^2 T^4}{288} \quad (30)$$

A similar, but more involved, calculation yields the result for  $\delta P_3(T)$  in the limit  $T \gg m$  [48],

$$\delta P_3(T) \simeq -\frac{e^3 T^4}{36\sqrt{3}\pi}. \quad (31)$$

At high temperatures, the ratio

$$\frac{\delta P_2(T)}{\delta P_3(T)} \simeq \frac{1}{e} \frac{\sqrt{3}\pi}{2} \simeq 11, \quad (32)$$

while both the  $e^2$  and the  $e^3$ -terms are exponentially suppressed for  $T \ll m$ . Therefore, to good approximation, we can neglect  $\delta P_3(T)$  for all  $T$ . For  $T \gg m_e$ ,  $\delta g_\rho = -25e^2/16\pi^2$ .

From the standard thermodynamic relation  $\rho = -P + T(\partial P/\partial T)$  we can find the thermodynamic correction to the energy density,  $\rho = \rho_0 + \delta\rho$ , where the standard density  $\rho_0$  may be written in terms of the density-weighted effective number of relativistic degrees of freedom,  $\rho_0 = (\pi^2/30) g_\rho T^4$ . The change in the density can be written

$$\delta g_\rho = \frac{30}{\pi^2 T^4} \left( -\delta P + T \frac{\partial}{\partial T} \delta P \right) \xrightarrow{T \gg m_e} -\frac{25}{16\pi^2} e^2. \quad (33)$$

Figure 14 shows  $\delta g_\rho$  and  $\delta g_P$  as a function of temperature.

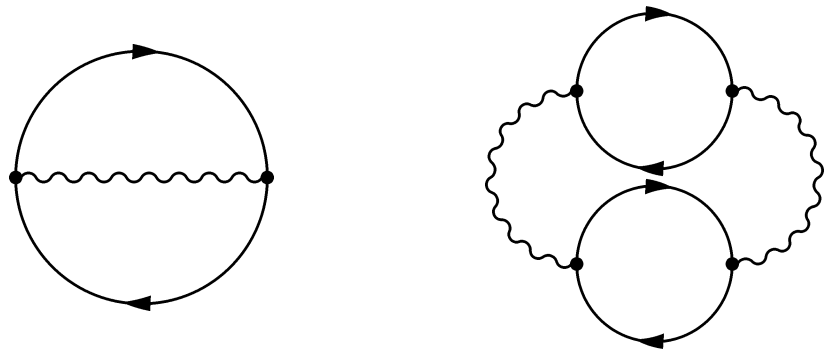


Figure 13: Feynman diagrams that contribute to the correction to the equation of state of the electromagnetic plasma. The left diagram produces the order  $e^2$  correction, while the right diagram is the smaller  $e^3$  correction.

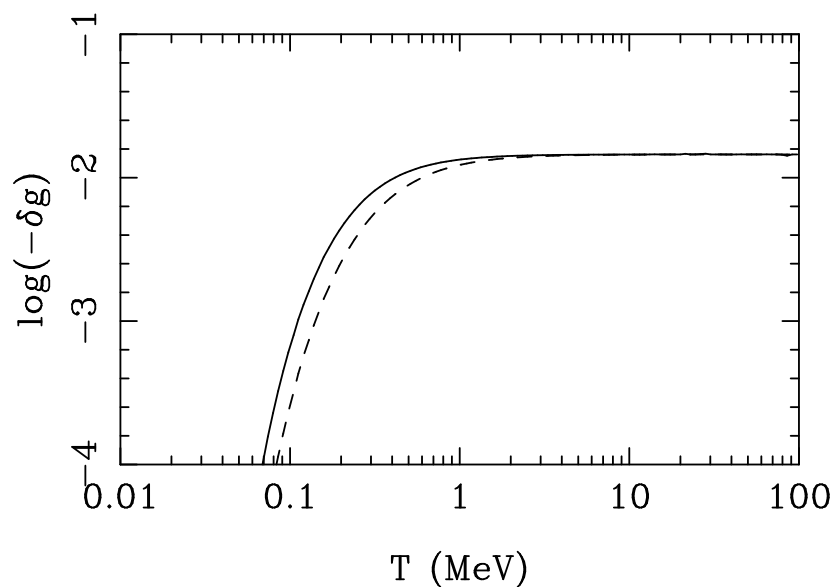


Figure 14: Finite-temperature QED change in pressure-weighted ( $g_P$ , solid line) and density-weighted ( $g_\rho$ , dashed line) relativistic degrees of freedom.

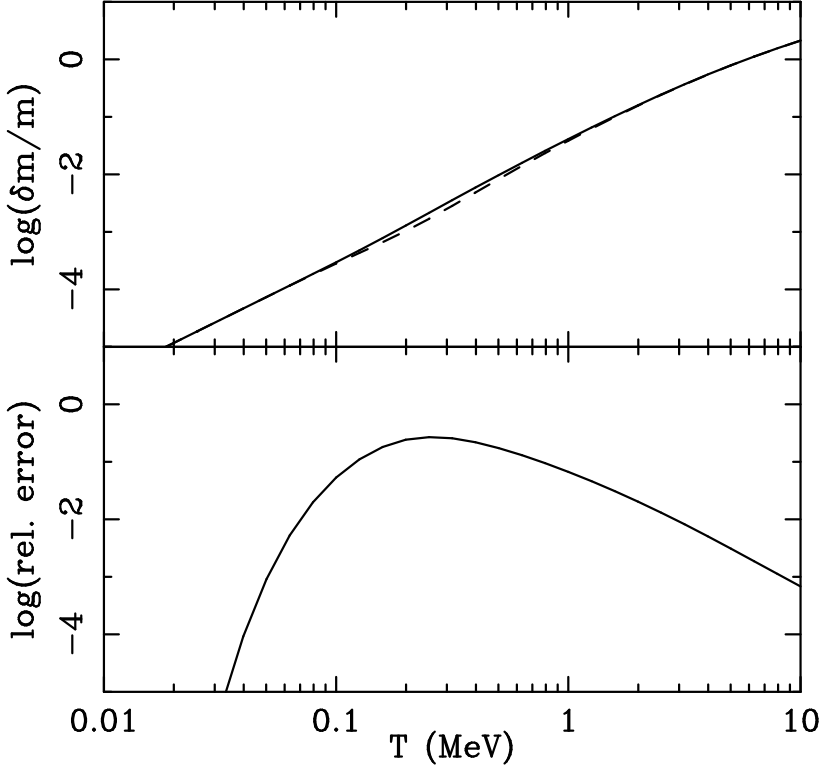


Figure 15: The top panel shows the finite-temperature QED correction to the electron mass as a function of temperature. The dashed curve neglects the  $p$ -dependent term, while the solid curve assumes  $p = 3T$ . The bottom panel shows the relative error due to not including the  $p$ -dependent term. This error, which is a ten percent correction to the correction, can be safely neglected.

The finite-temperature QED correction to the pressure is a change in the dispersion relation of the electrons which can be attributed to a change in the electron mass:

$$E^2 = p^2 + m^2 + \delta m^2. \quad (34)$$

The formula for  $\delta m^2$  follows from the definition of the pressure correction [48].

$$\begin{aligned} \delta m^2(p, T) = & \frac{e^2 T^2}{6} + \frac{e^2 T^2}{\pi^2} \int_x^\infty du \frac{k_u}{u} \frac{1}{e^u + 1} \\ & - \frac{e^2 m^2 T}{2\pi^2 p} \int_x^\infty du \ln \left| \frac{p_u + k_u}{p_u - k_u} \right| \frac{1}{e^u + 1}, \end{aligned} \quad (35)$$

where  $x = m_e/T$ ,  $k_u = \sqrt{u^2 - x^2}$  and  $p_u = p/T$ . Figure 15 shows the finite-temperature QED correction to the electron mass as a function of temperature. Figure 16 shows the effect of the shift in the electron's mass on the  $n \leftrightarrow p$  rates. The lower curves indicate the error due to not including the momentum-dependent part of the mass correction. For our calculations, the error is negligible and we neglect the  $p$ -dependent term in the mass correction formula.

The final effect of the thermodynamic corrections is a change in the neutrino-to-photon temperature ratio. This can be derived starting with the expression for  $\delta P(T)$  and tracking the entropy

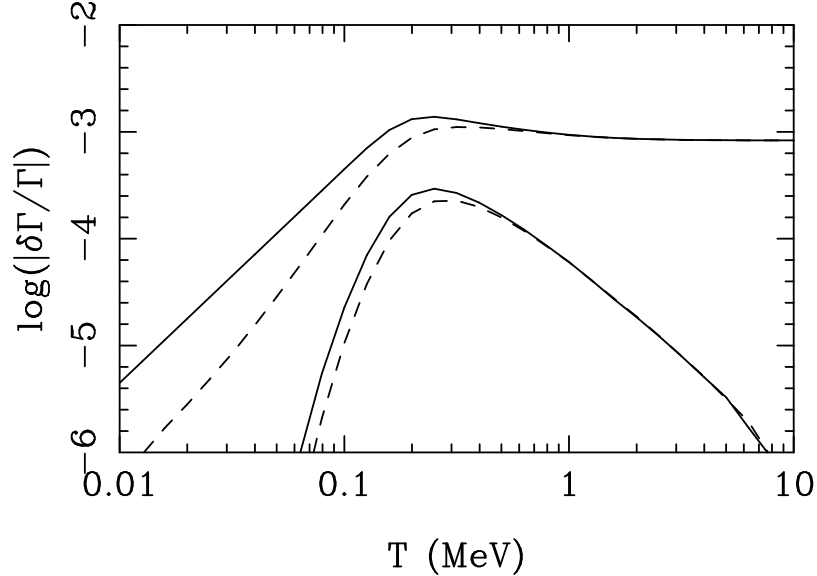


Figure 16: The top curves show the effect of the finite-temperature electron-mass correction on the weak rates. The solid curve is for  $n \rightarrow p$  and the dashed curve is for  $p \rightarrow n$ . The bottom curves show the error due to not including the  $p$ -dependent term in the mass correction formula.

density of the neutrinos and other particles. Let  $s_\nu$  be the entropy density of neutrinos and  $s_{\text{EM}}$  be the combined entropy density of the electrons, positrons and photons:

$$s_\nu = \frac{P_\nu + \rho_\nu}{T_\nu} = \frac{7\pi^2}{30} T_\nu^3, \quad (36)$$

$$\begin{aligned} s_{\text{EM}} &= \frac{P_{e^\pm} + \rho_{e^\pm} + P_\gamma + \rho_\gamma}{T} \\ &= T^3 \left[ \frac{4\pi^2}{45} + \frac{2}{3\pi^2} \int_x^\infty du \frac{\sqrt{u^2 - x^2}}{e^u + 1} (4u^2 - x^2) + \frac{\pi^2}{90} (\delta g_P + 3\delta g_\rho) \right]. \end{aligned} \quad (37)$$

In the limit that the neutrinos are completely decoupled, the two entropies per comoving volume are separately conserved:  $s_\nu a^3, s_{\text{EM}} a^3 = \text{constant}$ , where  $a$  is the scale factor. The small residual coupling of the neutrinos to the electromagnetic plasma leads to a correction of about  $\sim 0.1\%$  [27], discussed below, which can be ignored here. At high temperature we have

$$\left. \frac{s_{\text{EM}} a^3}{s_\nu a^3} \right|_{T \gg m_e} = \frac{22}{21} + \frac{1}{21} [\delta g_P(T) + 3\delta g_\rho(T)] \simeq \frac{22}{21} \left( 1 - \frac{25}{88} \frac{e^2}{\pi^2} \right), \quad (38)$$

while for all temperatures,

$$\frac{s_{\text{EM}} a^3}{s_\nu a^3} = \left( \frac{T}{T_\nu} \right)^3 \left[ \frac{8}{21} + \frac{20}{7\pi^4} \int_x^\infty du \frac{\sqrt{u^2 - x^2}}{e^u + 1} (4u^2 - x^2) + \frac{1}{21} [\delta g_P(T) + 3\delta g_\rho(T)] \right]. \quad (39)$$

Assuming that the neutrinos decouple at a temperature  $T_D \sim 2$  MeV  $\gg m_e$  and taking the ratio of entropies to be given by Eqn. (38), it follows that the ratio of the neutrino-to-photon temperature

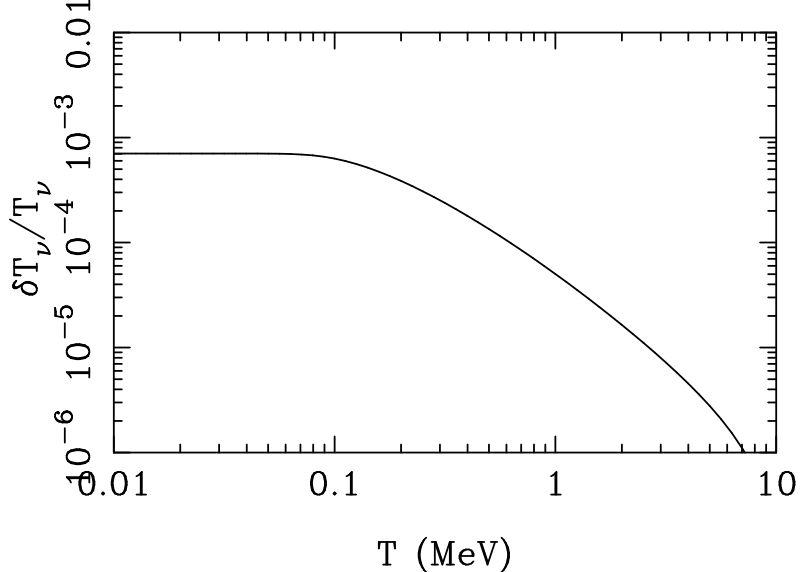


Figure 17: Relative finite-temperature QED change in the neutrino temperature, as a function of photon temperature. Note that the zero-temperature limit is altered from the standard value by about 0.08 %.

is

$$\left(\frac{T_\nu}{T}\right)^3 = \frac{\frac{4}{11} + \frac{30}{11\pi^4} \int_x^\infty du \frac{\sqrt{u^2 - x^2}}{e^u + 1} (4u^2 - x^2) + \frac{1}{22} [\delta g_P(T) + 3\delta g_\rho(T)]}{1 - \frac{25e^2}{88\pi^2}}, \quad (40)$$

$$\xrightarrow{T \ll m_e} \frac{4}{11} \left(1 + \frac{25e^2}{88\pi^2}\right) \simeq 1.002 \left(\frac{4}{11}\right). \quad (41)$$

The zero-temperature limit of the neutrino temperature photon temperature relation is altered <sup>3</sup>. This makes sense physically: the positive correction to the electron mass means that the electron-positron plasma has less entropy to give to the photons upon annihilation, and thus photons are heated less than they would be without the correction. Figure 17 shows the finite-temperature QED change in neutrino temperature versus photon temperature.

We incorporated the QED corrections to the equation of state into our code by changing the energy density, the electron mass in the weak-rate calculations and the neutrino temperature. The resulting change in  $Y_P$ ,  $\delta Y_P / Y_P = +0.043\%$  was found to be insensitive to  $\eta$  in the range,  $10^{-10} \leq \eta \leq 10^{-9}$ . Dicus, et al [15] attempted to calculate the thermodynamic corrections, and found  $\delta Y_P / Y_P = -0.04\%$ , but only included the effect of the electron mass on the weak rates. Heckler *estimated* the effect on  $Y_P$  and found  $\delta Y_P / Y_P = +0.06\%$ . (It should be noted that his value for the change in neutrino temperature was incorrect.) In any event, the thermodynamic correction to  $Y_P$  is small.

---

<sup>3</sup>This expression differs somewhat from the result obtained by Heckler [23]. He now agrees with our result

## 4.2 Incomplete Neutrino Decoupling

The standard code assumes that neutrinos decoupled completely before  $e^\pm$  annihilations. It has been pointed out that this assumption is not strictly valid [15]. Neutrinos are “slightly coupled” when  $e^\pm$  pairs are annihilated, and hence share somewhat in the heat released. The first calculations [15, 49, 50] of this effect were “one-zone” estimates that evolved integrated quantities through the process of neutrino decoupling. More refined “multi-zone” calculations tracked many energy bins, assumed Boltzmann statistics and made other approximations. [27, 51]. The latest refinements have included these small effects as well [52, 53, 54]. Fields et al [55] incorporated the slight effect of the heating of neutrinos by  $e^\pm$  annihilations into the standard code and found a shift in  ${}^4\text{He}$  production,  $\delta Y_P = +1.5 \times 10^{-4}$ , which is insensitive to  $\eta$  for  $10^{-10} \leq \eta \leq 10^{-9}$ .

## 5 Summary

All of the physics corrections we investigated have been studied elsewhere. However, not all of them have been implemented in a full code; some have been implemented incorrectly; and there have been changes in some of the physics corrections. Further, the issue of numerical accuracy of the standard code has not been comprehensively and coherently addressed. Finally, the corrections have been implemented in a patchwork fashion, so that the users of many codes do not know which corrections are in, which are out, and which may be double counted (e.g., by adding the numerical correction and running a small stepsize). As noted earlier, the results of a number of BBN codes gave a 1% spread in the prediction for  $Y_P$  with the same value of  $\eta$  and  $\tau_n$ .

The goal of this work was a calculation of the primordial  ${}^4\text{He}$  abundance to a precision limited by the uncertainty in the neutron mean lifetime,  $\delta\tau_n = \pm 2 \text{ sec}$ , or  $\delta Y_P/Y_P \simeq 0.2\%$ , with reliable estimates of the theoretical error. To achieve this goal we created a new BBN code, designed, engineered and tested to this numerical accuracy. To this baseline code we added the microphysics necessary to achieve our accuracy goal – Coulomb and zero-temperature radiative corrections, finite-nucleon-mass corrections, finite-temperature radiative corrections, QED thermodynamical corrections, and the slight heating of neutrinos by  $e^\pm$  annihilations. These corrections – coincidentally all positive – increase the predicted  ${}^4\text{He}$  abundance by  $\delta Y_P = 0.0049$  or 2%. Table 5 summarizes these corrections for  $\eta = 5 \times 10^{-10}$ . For each physical or numerical effect, we have been careful to control the error in  $Y_P$  introduced by approximations or inaccuracies to be well below 0.1%. With confidence we can state that the total theoretical uncertainty is less than 0.1%.

Summarizing our work in one number

$$Y_P(\eta = 5 \times 10^{-10}) = 0.2462 \pm 0.0004 \text{ (expt)} \pm < 0.0002 \text{ (theory)}. \quad (42)$$

Further, the precise value of the baryon density inferred from the Burles-Tytler determination of the primordial D abundance,  $\Omega_B h^2 = 0.019 \pm 0.001$  [56, 57], leads to the prediction:  $Y_P = 0.2464 \pm 0.0004 \text{ (expt)} \pm 0.0005 \text{ (D/H)} \pm < 0.0002 \text{ (theory)}$ .

Finally, we give two fitting formulae for our high-accuracy  ${}^4\text{He}$  predictions. The first, is accurate to better than 0.05% and is valid for  $10^{-10} \leq \eta \leq 10^{-9}$ ,  $N_\nu = 3.00$  and  $880 \text{ sec} \leq \tau_n \leq 890 \text{ sec}$ . In

	$Y_P$	Cumulative		Effect Alone	
		$\delta Y_P (\times 10^{-4})$	$\delta Y_P / Y_P (\%)$	$\delta Y_P (\times 10^{-4})$	$\delta Y_P / Y_P (\%)$
Baseline	0.2414				
Coulomb and $T = 0$ radiative	0.2445	+31	+1.28	+31	+1.28
finite mass	0.2457	+43	+1.78	+12	+0.50
finite $T$ radiative	0.2460	+46	+1.90	+3	+0.12
QED plasma	0.2461	+47	+1.94	+1	+0.04
residual $\nu$ -heating	0.2462	+49	+2.00	+1.5	+0.06

Table 5: Summary of results. For absolute numbers we have picked  $\eta = 5.0 \times 10^{-10}$ . By baseline we mean the results of our BBN code without any of the physics effects listed, and with small numerical errors.

terms of  $\zeta \equiv 10 + \log_{10} \eta$ ,

$$\begin{aligned}
 Y_P(\zeta, \tau_n) &= Y_P(\zeta, 885.4 \text{ sec}) + (\tau_n - 885.4 \text{ sec}) \delta Y_P(\zeta), \\
 Y_P(\zeta, 885.4 \text{ sec}) &= (a_0 + a_1 \zeta + a_2 \zeta^2 + a_3 \zeta^3 + a_4 \zeta^4), \\
 \delta Y_P(\zeta) &= (b_0 + b_1 \zeta + b_2 \zeta^2 + b_3 \zeta^3 + b_4 \zeta^4)
 \end{aligned} \tag{43}$$

where the coefficients  $a_i, b_i$  are given by

$$\begin{aligned}
 a_0 &= 0.22292, & a_1 &= 0.05547, & a_2 &= -0.05639, \\
 a_3 &= 0.04587, & a_4 &= -0.001501 \\
 b_0 &= 2.082 \times 10^{-4}, & b_1 &= 0.535 \times 10^{-4}, & b_2 &= -2.856 \times 10^{-4}, \\
 b_3 &= 4.672 \times 10^{-4}, & b_4 &= 2.420 \times 10^{-4}.
 \end{aligned} \tag{44}$$

The second fitting formula is accurate to 0.5% and is valid for  $10^{-10} \leq \eta \leq 10^{-9}$ ,  $880 \text{ sec} \leq \tau_n \leq 890 \text{ sec}$ , and  $2.5 \leq N_\nu \leq 4.0$ .

$$Y_P(\zeta, \tau, N_\nu) = Y_P(\zeta, \tau, 3) + (N_\nu - 3) (c_0 + c_1 \zeta + c_2 \zeta^2 + c_3 \zeta^3 + c_4 \zeta^4), \tag{45}$$

where

$$\begin{aligned}
 c_0 &= 0.01276, & c_1 &= 0.00409, & c_2 &= -0.00703, \\
 c_3 &= 0.00571, & c_4 &= -0.00186.
 \end{aligned} \tag{46}$$

## Acknowledgements

The BBN code we described in this paper began as a project for a graduate course in cosmology. R.L. gratefully acknowledges the work of his Red Team colleagues, Moses Hohman, Mike Joffre, Russel Strickland and Craig Wiegert. Thanks to Gary Steigman for helpful conversations. This work was supported in part by the DOE (at Chicago and Fermilab) and by NASA at Fermilab through grant NAG 5-2788, and 5-7092.

## References

- [1] D.N. Schramm and M.S. Turner, Rev. Mod. Phys. **70**, 303 (1998).
- [2] J. Yang, M.S. Turner, G. Steigman, D.N. Schramm, and K.A. Olive, Astrophys. J. **281**, 493 (1984).
- [3] T.P. Walker et al., Astrophys. J. **376**, 51 (1991).
- [4] Y. Izotov and T.X. Thuan, Astrophys. J. **500**, 188 (1998).
- [5] Y. Izotov and T.X. Thuan, Astrophys. J. **497**, 227 (1998).
- [6] K. Olive and G. Steigman, Astrophys. J. Suppl. **97**, 49 (1995).
- [7] K. Olive, E. Skillman, and G. Steigman, Astrophys. J. Suppl. **483**, 788 (1997).
- [8] K. Olive, E. Skillman, and G. Steigman, Astrophys. J. **489**, 1006 (1997).
- [9] B.E.J. Pagel and A. Kazlauskas, MNRAS **256**, 49 (1992).
- [10] B.E.J. Pagel et al., MNRAS **255**, 325 (1992).
- [11] S. Sarkar, Rep. Prog. Phys. **59**, 1493 (1996).
- [12] C.J. Copi, M.S. Turner, and D.N. Schramm, Phys. Rev. D **55** (1997).
- [13] V.F. Schvartsman, JETP Lett. **9**, 154 (1969).
- [14] G. Steigman, D.N. Schramm, and J. Gunn, Phys. Lett. **66B**, 202 (1977).
- [15] D. Dicus et al., Phys. Rev. D **26**, 2694 (1982).
- [16] J.F. Donoghue and B.R. Holstein, Phys. Rev. D **28**, 340 (1983).
- [17] J.F. Donoghue and B.R. Holstein, Phys. Rev. D **29**, 3004 (1984).
- [18] P. Kernan, PhD thesis, Ohio State University, 1993.
- [19] R.F. Sawyer, Phys. Rev. D **53**, 4232 (1996).
- [20] I.A. Chapman, Phys. Rev. D **55**, 6287 (1997).
- [21] M.S. Smith, L.H. Kawano, and R.A. Malaney, Astrophys. J. Suppl. **85**, 219 (1993).
- [22] G. Fiorentini, E. Lisi, S. Sarkar, and F. L. Villante, Phys. Rev. D **58**, 063506 (1998).
- [23] A.J. Heckler, Phys. Rev. D **49**, 611 (1994).
- [24] D. Seckel, hep-ph/9305311 (1993).
- [25] G. Gyuk and M.S. Turner, astro-ph/9307025 (1993).

- [26] R.E. Lopez, M.S. Turner, and G. Gyuk, Phys. Rev. D **56** (1997).
- [27] S. Dodelson and M.S. Turner, Phys. Rev. D **46**, 3372 (1992).
- [28] C. Caso et al., Euro. Phys. J. **C3**, 1 (1998).
- [29] S. Arzumanov et al., in *V International Seminar on Interaction of Neutrons with Nuclei*, Dubna, 1997.
- [30] J. Byrne et al., Europhys. Lett. **33**, 187 (1996).
- [31] L. Kawano, Fermilab-pub-92/04-a, 1992.
- [32] N. Itoh, A. Nishikawa, S. Nozawa, and Y. Kohyama, Astrophys. J. **488**, 507 (1997).
- [33] R.V. Wagoner, W. Fowler, and F. Hoyle, Astrophys. J. **148**, 3 (1966).
- [34] R.V. Wagoner, Astrophys. J. **179**, 343 (1973).
- [35] J. Lara, astro-ph/9806057 .
- [36] W.H. Press, S.A. Teukolsky, W.T. Vetterling, and B.P. Flannery, *Numerical Recipes in C*, Cambridge University Press, Cambridge, 1990.
- [37] R.V. Wagoner and D.N. Schramm, Ann. Rev. Nucl. Part. Sci. **27**, 37 (1977).
- [38] L. Kawano, Fermilab-pub-88/34-a, 1988.
- [39] P.J. Kernan and L.M. Krauss, Phys. Rev. Lett. **72**, 3309 (1994).
- [40] L. Krauss and P. Romanelli, Astrophys. J. **358**, 47 (1990).
- [41] L.M. Krauss and P.J. Kernan, Astrophys. J. Lett. **432**, 79 (1994).
- [42] N. Hata et al., Phys. Rev. Lett. **75**, 3977 (1995).
- [43] S. Burles, K. Nollett, J. Truran, and M.S. Turner, astro-ph/9901157 (1999).
- [44] S. Weinberg, *Gravitation and Cosmology*, J. Wiley, New York, 1972.
- [45] D.H. Wilkinson, Nucl. Phys. A **377**, 474 (1982).
- [46] J. Cambier, J.R. Primack, and M. Sher, Nucl. Phys. B **209**, 372 (1982).
- [47] S. Esposito, G. Mangano, G. Miele, and O. Pisanti, 1998.
- [48] J.I. Kapusta, *Finite-Temperature Quantum Field Theory*, Cambridge University Press, Cambridge, 1989.
- [49] M. A. Herrera and S. Hacyan, Astrophys. J. **336**, 539 (1989).
- [50] N. C. Rana and B. Mitra, Phys. Rev. D **44**, 393 (1991).

- [51] A. D. Dolgov and M. Fukugita, Phys. Rev. D **46**, 5378 (1992).
- [52] N.Y. Gnedin and O.Y. Gnedin, Astrophys. J. **509**, 11 (1998).
- [53] S. Hannestad and J. Madsen, Phys. Rev. D **52**, 1764 (1995).
- [54] A. D. Dolgov, S. H. Hansen, and D.V. Semikoz, Nucl. Phys. B **503**, 426 (1997).
- [55] B. Fields, S. Dodelson, and M.S. Turner, Phys. Rev. D **47**, 4309 (1993).
- [56] S. Burles and D. Tytler, Astrophys. J. **499**, 699 (1998).
- [57] S. Burles and D. Tytler, Astrophys. J. **507**, 732 (1998).